Lymphatic endothelial cells produce M-CSF causing massive bone loss in mice

Wensheng Wang[1,2,*], **Hua Wang**[2,4,*], **Xichao Zhou**[2], **Xing Li**[2], **Sun Wen**[2], **Michael Dellinger**[5], **Brendan F. Boyce**[2,3], and **Lianping Xing**[2,3,#]

[1]The 1st affiliated hospital, Xinxiang Medical University, Xinxiang 453000, China

[2]Department of Pathology and Laboratory Medicine, University of Rochester Medical Center, USA

[3]Center for Musculoskeletal Research, University of Rochester Medical Center, USA

[4]Institute of Stomatology, Jiangsu Key Laboratory of Oral Diseases, Nanjing Medical University, Nanjing, China

[5]Department of Surgery, University of Texas Southwestern Medical Center, Dallas, TX, USA

Abstract

Gorham-Stout disease (GSD) is a rare bone disorder characterized by aggressive osteolysis associated with lymphatic vessel invasion within bone marrow cavities. The etiology of GSD is not known and there is no effective therapy or animal model for the disease. Here, we investigated if lymphatic endothelial cells (LECs) affect osteoclasts (OCs) to cause a GSD osteolytic phenotype in mice. We examined the effect of a mouse LEC line on osteoclastogenesis in co-cultures. LECs significantly increased RANKL-mediated OC formation and bone resorption. LECs expressed high levels of M-CSF, but not RANKL, IL-6 and TNF. LEC-mediated OC formation and bone resorption were blocked by an M-CSF neutralizing antibody or Ki20227, a inhibitor of the M-CSF receptor, c-Fms. We injected LECs into the tibiae of WT mice and observed massive osteolysis on X-ray and micro-CT scans. Histology showed that LEC-injected tibiae had significant trabecular and cortical bone loss and increased OC numbers. M-CSF protein levels were significantly higher in serum and bone marrow plasma of mice given intra-tibial LEC injections. Immunofluorescence staining showed extensive replacement of bone and marrow by podoplanin+ LECs. Treatment of LEC-injected mice with Ki20227 significantly decreased tibial bone destruction. In addition, lymphatic vessels in a GSD bone sample were stained positively for M-CSF. Thus, LECs cause bone destruction in vivo in mice by secreting M-CSF, which promotes OC formation and activation. Blocking M-CSF signaling may represent a new therapeutic approach for treatment of patients with GSD. Furthermore, tibial injection of LECs is a useful mouse model to study GSD.

[#]Corresponding author: Lianping Xing, Department of Pathology and Laboratory Medicine, 601 Elmwood Ave, Box 626, Rochester, NY 14642, USA. Phone (585) 273-4090, Fax (585) 756-4468, Lianping_xing@urmc.rochester.edu.
[*]These authors made equal contribution to this work.

Keywords

Gorham-Stout disease; lymphatic endothelial cells; M-CSF; osteoclasts; bone resorption

INTRODUCTION

Gorham-Stout disease (GSD) is a rare disorder characterized by massive osteolysis, also referred to as disappearing bone disease. GSD is usually accompanied by proliferative non-neoplastic thin-walled lymphatic vessels or sometimes blood vessels that invade bone tissues and replace local bone [1, 2]. GSD may occur in the skull, shoulder, ribs, spine, or any boney structure. It can develop in any age, and no gender-bias is found. But the most of reported cases are younger than 40 years old [3]. GSD could be diagnosed by X-ray, computed tomography, magnetic resonance imaging, and histopathological examination [1, 2].

The etiology of GSD is poorly understood and no animal models are currently available. In 1996, Devilin et al. reported serum from a GSD patient who has active disease markedly increased the formation of multinuclear cells and their resorbing capacity in cultures of normal human bone marrow cells. The GSD serum contains high IL-6 levels, but not IL-1, TNFα or PTH levels. IL-6 neutralizing antibody blocked GSD serum-induced osteoclast (OC) formation, suggesting that bone loss in GSD is likely due to IL-6 mediated OC activation[4]. In 1999, Moller et al reported 6 GSD cases with histopathological findings showing active OCs in the marrow, or even in deep Howship's lacunae [5]. Later studies indicated that increased OC formation in GSD is due to an increase in the sensitivity of OC precursors to humoral factors that promote OC formation and bone resorption [6]. Monocytes isolated from GSD patients have an invasive phenotype and produced osteoclastogenic and angiogenic factors, suggesting that cells in the myeloid lineage play an important role in the pathogenesis of GSD [7].

OCs are differentiated from the myeloid progenitor cells in the presence of M-CSF and RANKL, two essential factors for OC development. M-CSF binds to its receptor c-Fms, and M-CSF/c-Fms signal is required for survival of myeloid progenitor cells, thereby OC differentiation [8]. Under physiological condition, M-CSF and RANKL are mainly produced by cells in the osteoblast lineage. Other factors including TNF, IL-1 and IL-6 could promote OC formation, but they are not essential, and play a more important role in pathological bone loss, such as inflammation and cancers. Under these conditions, many cell types produce osteoclastogenic factors, including T and B lymphocytes [9, 10], and blood endothelial cells [11, 12]. However, the effect of lymphatic vessel endothelial cells on OC formation and function are not known. Lymphatic vessels play an important role in tissue homeostasis and immune cell transportation [13]. We reported that OC precursors and mature OCs produce lymphatic endothelial cell growth factor VEGF-C that enhances the bone resorbing capacity of mature OCs moderately via an autocrine mechanism. VEGF-C alone cannot induce OC differentiation [14]. OC-produced VEGF-C cannot be used to explain the massive bone loss in GSD patients because the effect of VEGF-C on OCs is small, and there are no lymphatic vessels within the bone marrow. Thus, during normal bone

remodeling, OC-produced endogenous VEGF-C is not sufficient to lead to lymphangiogenesis in the bone marrow. Other factors must be involved in mediating bone loss in GSD. In this study, we used both in vitro and in vivo approaches and demonstrated that lymphatic endothelial cells produce a large amount of M-CSF to promote osteoclastogenesis and bone resorption, indicating that M-CSF represents a new therapeutic target and perhaps a clinical biomarker for GSD patients.

MATERIALS AND METHODS

Cell lines and animals

A murine LEC cell line established from Freunds adjuvant–induced benign lymphangiomas was used [15](cells provided by Dr. S. Ran from the University of Illinois, Springfield, Illinois, USA). A mouse lung blood vessel endothelial cell line (BEC) was purchased from the Cell Bank of the Chinese Academy of Sciences (Shanghai, China). Osteoblast precursor cell line, MC-3T3 E1 cells, was used. Cells were cultured in α-minimal essential medium (α-MEM) supplemented with 10% fetal calf serum (FCS, JRH Biosciences, Lenexa, KS), 1% penicillin-streptomycin. WT C57BL/6 mice were purchased from Jackson Laboratories (Stock [#]000664). Unless otherwise stated, experiments were performed in 8–10-week-old mice. Both male and female mice were used and we did not notice obvious difference in LEC injection caused osteolysis between male and female mice. All the animals used in this study were approved by Animal Care and Use Committee of University of Rochester, USA or Nanjing Medical University, China.

Reagents and antibodies

c-Fms tyrosine kinase inhibitor, Ki20227 (N-[16]-N'-[1-(1,3-thiazole-2-yl)ethyl]urea) was purchased from AdooQ (Irvine, Cat[#]A11472-50). Mouse RANKL was purchased from Novoprotein (Cat[#]CR06). Reduced Matrigel was purchased from Corning (Cat[#]356230).PE-conjugated anti-mouse podoplanin (PDPN, Cat[#]127408), violet 605-conjugated anti-mouse CD115 (=c-Fms, Cat[#]135517), and Cy5.5-conjugated anti-mouse CD105 (Cat[#]120415) antibodies were purchased from Biolegend. Biotin-conjugated anti-mouse Lymphatic Vessel Endothelial Hyaluronan Receptor 1(LYVE-1, Cat[#]13-0443-80), FITC-conjugated anti-mouse CD31 (Cat[#]11-0311-81), APC-conjugated anti-mouse CD11b (Cat[#]17-0112-83) antibodies were purchased from eBioscience. Streptavidin-conjugated APC was purchased from BD Pharmingen (Cat[#]554067). Hamster anti-mouse PDPN (Abcam, Cat[#]ab11936), FITC-conjugated anti-mouse smooth muscle actin (Sigma, Cat[#]F3777), goat anti-mouse VEGFR3 (Cat[#]AF743) antibodies were purchased from R&D Systems. Anti-mouse Prox1 antibody (Cat[#]11-002) was purchased from AngioBio. Alexa flour 488-conjugated anti-goat (Cat[#]A11078) and Alexa flour 568-conjugated anti-hamster (Cat[#]A21111) antibodies were purchased from Invitrogen.

Primary lymphatic cell isolation

Extra-peritoneal membrane was cut from mice and digested with 1 mg/ml collagenase IV at 37°C for 1 hour with vortex per 10 min and stopped by adding 2% FBS in PBS. Digested cells were passed through Falcon 40 μm cell strainer (Corning, Cat[#]352340), centrifuged, and cell pellet was re-suspended and cultured with DMEM containing 15% FBS. Briefly,

after 4–6 days' culture, cells were detached with 0.25% Trpsin/EDTA and washed once with MACS buffer (phosphate-buffered saline (PBS), pH 7.2, 0.5% bovine serum albumin, and 2 mM EDTA) and incubated with PE-conjugated anti-mouse PDPN antibody at 4°C with rotation for 30min. After being washed with MACS buffer, cells were incubated with anti-PE-micro beads (Miltenyi BiotecInc, Cat#130-048-801) at 4°C with rotation for 30min. After wash with MACS buffer, cells were re-suspended with 500 µl MACS buffer and applied onto the prepared MS column(Miltenyi BiotecInc, Cat#130-042-201). Cells that were passed through the column were collected as PDPN– control cells. Column was then washed 3 times with MACS buffer and PDPN+ cells were pushed out from column with 1 ml MACS buffer. Cells were cultured on 10 cm dishes for several days and frozen down stocks for future use.

Tube formation assay

Phenol-red free, reduced growth factor matrigel was placed on ice to thaw overnight. Matrigel (150 µl) was added into a 48-well plate at 37ºC for 30 min for polymerization. LECs were washed once with PBS and harvested with 0.25% trypsin/EDTA (Invitrogen, Cat#25200-056). LECs (4×10^5) were loaded on polymerized matrigel for 4 hours at 37 ºC to form tube-like structures. Tubes were imaged under an inverted microscope. The number of tubes/well were analyzed with ImageJ and Angioquant software according to a published protocol [17].

Cell immunostaining

Cells were fixed with 4% PFA for 10 min, washed 3 times with PBS, and blocked with 10% goat serum (Victor, Cat#S-1000) in 0.2% PBST (0.2% Triton X-100 in PBS) for 1 hour at room temperature. After being washed 3 times with 0.2% PBST, cells were incubated with an anti-mouse Prox1 antibody (1:200) followed by Alexa flour 488 conjugated anti-rabbit antibody (1:500) at 4°C overnight. After 3 washes with 0.2% PBST, cells were mounted with Vector H-1000 (Vector, USA) and observed with fluorescent microscope (Olympus IX71).

Flow cytometry

Cells were harvested with 0.25% trypsin/EDTA, washed once with FACS buffer (2% fetal bovine serum in PBS) and stained with PE-conjugated anti-mouse PDPN, biotin-conjugated anti-mouse LYVE-1, FITC-conjugated anti-mouse CD31, Violet 605-conjugated anti-mouse c-Fms, APC-conjugated anti-mouse CD11b and Cy5.5-conjugated anti-mouse CD105 antibodies for 30 min at 4C. After being washed with FACS buffer, cells were fixed with 2% formalin in PBS and subjected to flow cytometric analysis (BD LSRII 12 color). Results were analyzed using the FlowJo7 software. Isotype IgG was used as the control.

Quantitative real time PCR

Total RNA was extracted from cells or long bones after removal of BM with TRIzol reagent (Invitrogen, Cat#15596018) following the manufacturer's instructions. Reverse transcription was performed to synthesize cDNA using M-MLV Reverse Transcriptase from 1µg total RNA according to manufacturer's manual (Invitrogen, Cat#28025-013). Quantitative real

time PCR was performed by using iQ SYBR Green supermix (Biorad, Cat[#]170-8882) and an iCycler real time PCR machine (Biorad). All the primers for quantitative PCR are listed in Table. RNA samples from 3 wells were analyzed to get mean for gene expression, and the same experiments were repeated at least 3 times. The relative expression levels of the genes of interest were presented as the CT value of each gene or fold changes over the housekeeping gene, gapdh.

M-CSF knockdown

M-CSF siRNA, a pool of 3 target-specific 19–25 nt siRNAs designed to knock down mouse M-CSF gene expression (Cat[#] sc-39394) and control siRNA (Cat[#] sc-37007) were purchased from Santa Cruz. LECs were transfected with 20nM M-CSF or control siRNA using Lipofectamine™ RNAiMAX lipid reagent (Invitrogen, CA, USA) as described in manufacturer's instructions. Cells were collected at 60 hrs post siRNA transfection, and expression of M-CSF was determined qPCR. Medium was changed to fresh α-MEM +10%FBS for 24 hrs and LEC conditional media (CM) that were collected.

Osteoclast formation and resorption assays

Bone marrow (BM) cells were flushed from mouse femora and tibiae and cultured with α-MEM containing 10% FCS and M-CSF supernatant (1:50 dilution) from an M-CSF-producing cell line CMG14–12[18] or CM from LECs, MC-3T3 osteoblast precursors, or BECs, that was collected during the 2-day-culture period. Then RANKL (10 ng/ml) was added into medium and cells were cultured for another 3–5 days. When optimal osteoclast (OC) formation was observed under an inverted microscope, based on assessment of multinucleated cells formation, the cell culture was stopped. The cells were fixed and stained for tartrate-resistant acid phosphatase (TRAP) activity to identify OCs. TRAP^{+} cells containing   3 nuclei were counted as OCs. For functional studies, BM cells were cultured on bone slices under the same conditions for 10 days as described above. Bone slices were stained for TRAP activity and OCs were counted. Then osteoclasts were removed and bone slices were stained with 0.1% toluidine blue to visualize resorption pits. The area of pits was quantified and data were expressed as area of pits (mm^2)/slice.

Osteoblast assays

Mouse bone-derived mesenchymal progenitor cells (MPCs) were used. MPCs were generated, as we described previously [19]. Briefly, long bones were flushed several times with PBS, cut into small pieces, and cultured in a plastic dish for 3 days in α-MEM culture medium containing 10% FCS. The bone pieces were transferred into a clear dish as passage 1 and continually cultured for another 7 days to allow cell growth to confluence. Third passage MPCs were seeded into 96-well-plate at 2000 cells/well. 24 hours later, LEC CM was co-cultured with MPCs in osteoblast-inducing medium containing 50μg/ml ascorbic acid and 10 mM β-glycerophosphate for 48 hours. ALP staining was performed using the 1-step NBT/BCIP reagent (Thermo Scientific).

Enzyme-Linked Immunosorbant Assay (ELISA)

For BM plasma, BM cells were flushed from tibia with 0.8 ml PBS containing 0.2% BSA and centrifuged (2000g, 4 °C for 10 min). BM plasma was collected and stored at −80°C. For serum, blood was harvested via the cardiac puncture, and left at room temperature for 2 hours to clot and then centrifuged for 20 min at 2000g. Serum was harvested and stored at −80°C. For LEC CM, LECs (10^6) were cultured in 10 cm culture dishes overnight. Once LECs completely attached to culture dishes, fresh culture medium (α-MEM containing 10% fetal calf serum) was changed. CM was collected after 2 and 4 days cultures, mixed together, centrifuged, and stored at −80°C. M-CSF protein levels were measured using a Mouse M-CSF Quantikine ELISA Kit (R&D, Cat#MMC00) according to manufacturer's instructions. OD values were measured by iMark microplate reader (Biorad).

Intra-tibial injection of LECs and X-ray analysis

LECs or BECs were detached with 0.25% Trpsin/EDTA after cells reached 60%~70% confluence and re-suspended in PBS. Cell viability (90%) was confirmed by trypan-blue dye exclusion test. Mice were anesthetized using katemine. A 25-gauge needle was inserted into the bone marrow cavity via the tibial crest, epiphysis and growth plate, and 5×10^5 viable cells in 5μl was injected into the right tibia. Left tibia was injected PBS as control. X-ray (Faxitron) was used to confirm that needle was inserted into tibia. Mice were X-rayed (26 kV for 5 seconds) every week to monitor the development and progression of osteolytic lesion. The radiographs were captured with Faxitron DX software and saved as JEPG files.

Micro-computed tomography

Two weeks after LEC injection, mice were anesthetized with isoflurane and were scanned at high resolution (10.5 μm) on a VivaCT40 micro-computed tomography scanner (Scanco Medical, Bassersdorf, Switzerland) using an integration time of 300 ms, energy of 55 peak kilovoltage, and intensity of 145 μA. The three-dimensional images were generated using a constant threshold of 275 for all samples. For each sample, bone volume fraction, trabecular number, trabecular thickness, trabecular separation, and connectivity density were measured by μCT Evaluation program V6.5–1.

Histology and analysis

Legs were fixed in 10% buffered formalin, decalcified in 10% EDTA for 3 weeks, and embedded in paraffin. Sections (4μm thick) were stained with H&E for general histology and for TRAP activity to identify OCs. OC numbers per mm bone surface and bone volume/ tissue volume (BV/TV %) were assessed using an Osteometrics image analysis software system. Each data point was mean of 3 levels (50μm apart) from one sample.

Immunofluorescence staining

1) Mouse samples. Legs were fixed in 10% formalin, decalcified in 10% EDTA, and embedded OCT compound ((Tissue Tek, Sakura). Frozen sections were cut using a Leica CM1850 cryostat (Leica, German). For immunofluorescence (IF) staining, sections were blocked with 10% normal horse serum and 0.2% Triton X-100 in PBS for 1 hour and then

stained overnight with hamster anti-PDPN (ab11936, 1:200) and rat anti-endomucin (sc-65495, 1:50)antibodies at 4°C. After rinsing with PBS for 15 min, tissues were incubated with goat anti-hamster Alexa Fluor 568 and goat anti-rat Alexa Fluor 488(Invitrogen, 1:400) at room temperature. Slides were mounted with mounting medium containing DAPI (Vector), and images were taken withVS120 Virtual Slide Microscope (OLYMPUS). 2) Human samples. Un-stained paraffin sections from GSD patients were incubated at 60°C for one hour, transferred to xylene and hydrated by sequential immersion in ethanol, 95% ethanol, 75% ethanol and finally water. Antigens were unmasked in DAKO antigen retrieval solution (S1699, DAKO) for 30 min. Non-specific binding was blocked with 5% normal house serum for 30 min at room temperature. Rabbit anti-LYVE1 (ab14917, 1:200) and mouse anti M-CSF (sc-365779, 1:50) antibodies were added to the slides and incubated at room temperature in a humid chamber overnight. On the next day, slides were washed with PBS, and incubated with goat anti-rabbit Alexa Fluor 568 and goat anti-mouse Alexa Fluor 488(Invitrogen, 1:400) at room temperature. Slides were washed with PBS and mounted with Prolong gold antifade with DAPI (P36931, Life technologies). Representative pictures were taken with a Zeiss Axiocam digital Camera (Carl Zeiss) and a Zeiss Axioplan 2 microscope.

Statistical analysis

Statistical analyses were performed with GraphPad software. All of experiments were performed at least twice with similar results. Data are presented as mean ± S.E. Analyses between 2 groups were used unpaired student t-test. When comparing the difference among >2 groups, one-way analysis of variance was used followed by Dunnett's test and/or Bonferroni's test. *p* values <0.05 were considered to be statistically significant.

RESULTS

Lymphatic endothelial cells stimulate osteoclast formation

We used an established mouse lymphatic endothelial cell (LEC) line [15]. To further characterize these cells, we first examined the growth curve and demonstrated that the doubling time is about 16.09 ± 1.58 hours. Since one characteristic of endothelial cells is the ability to form tube-like structures *in vitro*, we examined the tube-forming capacity and demonstrated that LECs could form tube-like structures on a Matrigel culture. The homeobox transcription factor, Prox1, is essential for the development of LECs [20]. We demonstrated that these LECs were stained positively for Prox1 that is localized in the nucleus. Furthermore, flow cytometric analysis indicated that most of LECs expressed stromal cell marker CD105 and LEC markers PDPN and VEGFR3 [21–25]. Some of them expressed LYVE-1 and none expressed markers for the blood endothelium CD31 or markers for myeloid cells, c-Fms and CD11b. The gene expression profile revealed that LECs expressed high levels of genes related to LEC formation and functions. These data (not shown) indicate that this cell line has properties of LECs.

To determine if LECs adversely affect the function of osteoclasts (OCs) or osteoblasts, resulting in GSD osteolytic phenotype, we examined the effect of LECs on OC and osteoblast differentiation in co-cultures. We co-cultured BM cells from WT C57BL/6 mice

with different numbers of LECs in the presence of RANKL or M-CSF, but not both, to determine if LECs support OC formation by producing RANKL or M-CSF. In the presence of RANKL, OC formation was observed when BM cells were co-cultured with lower numbers of LECs. In contrast, when BM cells were co-cultured with LECs in the presence of M-CSF, no OC was formed (data not shown). To determine if LEC-mediated OC formation requires direct cell to cell contact, we cultured BM cells with conditioned media (CM) from LECs. In the absence of RANKL, LEC CM did not cause OC formation while in the presence of RANKL, LEC CM promoted OC formation, starting at 10% and peaked at 20% (Figure 1A). The OC number formed in the presence of 20% LEC CM+RANKL was similar to the OC number formed in the presence of M-CSF +RANKL (OC numbers/well: 187.3±4 vs. 213.3±5). To further indicate high osteoclastogenic potential of LECs, we cultured BM cells with CM from MC-3T3E1 osteoblast precursors or BECs in the presence of RANKL. LEC CM induced much more OC formation than CM from other cell types (Figure 1B). To confirm the function of LEC CM-induced OCs, we performed bone resorption assays and demonstrated that they resorbed a similar degree of bones as OCs that was formed in the presence of M-CSF (Figure 1C). In contrast, we did not find a significant effect of LECs on osteoblast differentiation (Figure 1D).

LECs produce M-CSF and M-CSF neutralizing antibody blocks LEC-mediated osteoclastogenesis

The results above strongly suggest that LECs produce M-CSF to promote OC formation. We reported previously that M-CSF increases the number of CD11b$^+$/Gr-1$^{-/lo}$OC precursors in vitro [26]. To examine if LEC CM has a similar effect as M-CSF, we cultured WT BM cells with M-CSF, 20% LEC CM, or α-MEM for 3 days and examined the percentage of OC precursors by flow cytometry. As we previously reported, primary BM cells contained about 10% OC precursors and M-CSF increased their percentage to about 90% after 3-day culture. Impressively, LEC CM increased the percentage of OC precursors to a degree similar to M-CSF (Figure 2A). To further demonstrate this point, we used more cell surface markers, including CD45+/ckit+/c-fms+, for OC precursors. LEC CM increased the percentage of CD45+/ckit+/c-fms+ OC precursors to a similar degree as M-CSF (Figure 2A). Apart from M-CSF and RANKL, TNFα is another cytokine that can induce OC formation *in vitro* and high IL-6 levels have been reported in some of GSD patients [4, 27–29]. We thus examined the expression levels of *m-csf*, *rankl*, *tnf-α*, and *il6* mRNA in LECs by qPCR. LECs expressed very high levels of *m-csf*, but not *rankl*, *tnf-α*, and *il6,* which was indicated by the low cycle numbers of *m-csf* (21 ±0.5 vs. 34.5 ± 0.08 of *rankl,* Figure 2B). We did not detect expression of *il-1*, another OC cytokine, in LECs. ELISA of LEC CM confirmed that it contained high levels of M-CSF protein, which reached about 30 ng/ml (Figure 2C). More importantly, M-CSF neutralizing antibody blocked LEC CM-induced-OC formation and bone resorption while isotype IgG control had not effect (Figure 2D). To determine if M-CSF from LECs to promote OC formation or if there are additional soluble factors augment the M-CSF production by LEC cells, we knocked down M-CSF in LECs using a siRNA approach. Compared to control siRNA-transfected cells, CM from M-CSF siRNA-transfected LECs supported significantly less OC formation (Figure 2E).

To determine whether osteoclastogenic effect is a general feature of LECs or this specific cell line, we isolated primary LECs from peritoneal membrane using an anti-PDPN antibody according to a published protocol [21, 30, 31]. We first demonstrated that these PDPN+ cells expressed LEC surface markers including PDPN, LYVE-1 and VEGFR3, and stromal cell marker CD105, but not myeloid marker CD115. Some of them also expressed BEC marker CD31 (Figure 2F). Similar to our LEC cell line, PDPN+ cells expressed high levels of M-CSF, but not RANKL mRNA (Figure 2G). We then compared osteoclastogenic potential of PDPN+ LEC CM with CM of PDPN− cells that were isolated in the same time. PDPN+ LEC CM stimulated 2–3-fold more OC formation than PDPN− cell CM (Figure 2H). Accordingly, PDPN+ LEC CM contains a similar level of M-CSF proteins by ELISA (14.8±1.51 vs. 5.13±1.07 ng/ml in CM from PDPN− cells, Figure 2I).

Intra-tibial injection of LECs results in osteolysis, associated with elevated M-CSF levels in recipient mouse bone marrow

To determine if LECs could result in osteolytic lesion *in vivo*, we injected LECs into the tibiae of WT C57BL/6 female mice and examined bone destruction by X-ray, micro-CT, and histology, and M-CSF levels in the peripheral blood and BM of recipient mice by ELISA at 2 weeks post-LEC administration. X-ray examination displayed severe osteolysis in tibia received LEC injection compared to PBS-injected contra-lateral tibia of the same mouse (Figure 3A). Micro-CT scanning revealed obvious bone destruction at the LEC injected tibiae (Figure 3B). ELISA results indicated that mice received LECs had significantly higher serum M-CSF levels (1.82±0.3 ng/ml vs. 1.33±0.1ng/ml, p<0.05). BM plasma collected from LEC-injected tibia had 2–3 fold higher M-CSF than that from the contralateral tibia that received PBS (58.88±5.87 pg/ml vs. 21.60±11.18 pg/ml, p<0.05) (Figure 3C). H&E-stained paraffin sections showed that tibial bone that received LEC injection had trabecular bone loss and cortical bone erosion, which is associated with increased TRAP+ OCs (Figure 3D&E). We did not detect increased OC numbers or change of bone volume in the PBS-injected contra- lateral tibia of the same mouse. We also performed intra-tibial injection of BECs using the same protocol as LEC injection and did not find bone loss in BEC-injected tibiae (Figure 3F&G).

The c-Fms inhibitor suppresses LEC-induced osteolysis and osteoclastogenesis

M-CSF signals through its receptor c-Fms, and several c-Fms inhibitors have been used in pre-clinical animal models to inhibit tumor-produced M-CSF on tumor growth and bone destruction [32]. For instance, Ki20227, a c-Fms tyrosine kinase inhibitor, suppresses osteoclast differentiation and tumor growth in a mouse osteosarcoma model [32]. Thus, if LEC-induced osteolysis is medicated by M-CSF, Ki20227 should be able to block or attenuate the effect of LECs *in vivo*. To test this, we first examined if Ki20227 inhibits OC formation in the presence of LEC CM in the OC formation assay and demonstrated that Ki20227 suppressed OC formation in a dose-dependent matter, starting at 1 nM and peaked at 5 nM (Figure 4A). We then treated mice that had received LEC injection with Ki20227 (40mg/kg/day) or PBS control daily, starting at day 2 post-LEC administration, for 2 weeks. X-ray examination showed that Ki20227 reduced LEC-medicated osteolysis (Figure 4B). Micro-CT of tibiae indicated that Ki20227-treated mice have higher bone volume (Figure 4C), which is confirmed by histology (Figure 4D). To determine how fast LECs could lead

to osteolytic lesion after they have been injected into the BM cavity, we examined bones at 7, 10, 13 and 16 days post-LEC administration. Radiographs detected multiple osteolytic lesions in LEC-injected legs at 7 days, which spread to destroy the medullary bone, and then the cortical bone. H&E- and TRAP-stained sections showed trabecular bone loss and cortical bone erosion at 7 days, resulting in almost complete disappearance of cortical bone at 16 days. These lesions were associated with massive OC formation (data not shown).

LECs maintain their capacity to express podoplanin

To determine if injected LECs still express PDPN and M-CSF after they have resided in the BM and if they could form lymphatic vessels, we stained frozen tibial sections from mice that were killed at 19 days post-LEC injection. TRAP staining confirmed massive increased TRAP+ OCs. An adjacent section that was stained with anti-PDPN and anti-MCSF antibodies indicates groups of PDPN+ cells, M-CSF+ cells and PDPN+/M-CSF+ cells, but not PNPD+ lymphatic vessel-like structures (Figure 5A). To examine the effects of LEC injection on endogenous M-CSF and RANKL expression, we examined their levels in crashed bones after bone marrow was removed and found markedly increased M-CSF mRNA and slightly increased VEGF-C levels, but no change in RANKL expression (Figure 5B). To determine what happens to the BM composition after LEC injection, we stained performed with surface markers for myeloid cells and subjected them to flow analysis. LEC injection led to a decreased percentage of myeloid cells (Figure 5C).

Lymphatic endothelial cells in bone samples from a GSD patient express M-CSF

To determine if LECs of lymphatic vessels in GSD patients express M-CSF *in vivo*, we initially attempted to obtain tissue blocks from Dr. Erik A. Eklund who was funded by the Lymphatic Malformation Institute to centralize a tissue bank with specimens from GSD patients around the world. Since GSD is a rare disease, only 29 cases have been collected since the bank was funded. Among these, six cases have bone specimens, only one of which contains useful bone marrow tissue for immunofluorescence staining. We found that in this case, lymphatic vessels in the periosteum were stained strongly positive for M-CSF and LYVE-1, but no lymphatic vessels were detected within the bone marrow of this specimen (data not shown). Recently, we obtained bone samples from another case of GSD patient. In this new case, we observed numerous lymphatic vessels within the bone marrow cavity. All lymphatic vessels were stained positively for LYVE-1, some of which were also stained positively for M-CSF (Figure 6). The percentage of LYVE-1/M-CSF double positive vessels is 60±13% when we counted vessels from 3 areas in this sample. However, we did not observe increased OCs in both cases.

DISCUSSION

In this study, we demonstrated that lymphatic endothelial cells (LECs) produce high levels of M-CSF and stimulate osteoclast formation. Intra-tibial injection of LECs into WT C57BL/mice leads to a GSD-like phenotype, e.g. massive osteolysis, osteoclastogenesis and bone destruction attenuated by an M-CSF/c-Fms signal inhibitor. Thus, LEC-produced M-CSF is the key therapeutic target for osteolyic lesion in GSD and intra-tibial injection of LECs represents a useful mouse model for GSD.

It is well known that osteolysis in bone of GSD patients is often accompanied by localized proliferation of lymphatic or blood vessels [33–35]. However, whether and how lymphatic vessels affect bone has not been studied previously. Bone mass is maintained by a balance between bone resorption and formation. We found that LECs do not affect osteoblast differentiation *in vitro*, rather strongly promote osteoclast formation and function, indicating that bone loss phenotype in GSD is mainly due to LEC-mediated osteoclastic bone resorption. Increased VEGF-A, VEGF-C and IL-6 in serum of GSD patients have been reported [36], all of which have the ability to increase osteoclast function *in vitro* in the presence of RANKL and M-CSF, two essential factors for osteoclastogenesis [27, 28]. However, the sources of these factors have not well studied. Our finding that LEC express high levels of M-CSF raises 2 new points for GSD pathogenesis. One is that LECs are an important source of osteoclastogenic cytokines. Another is that M-CSF is a critical pathogenic factor for GSD.

Osteoclasts are derived from precursors in the myeloid/monocyte lineage. M-CSF is essential for survival and proliferation of this lineage cells. M-CSF also auto-amplifies its own signal by stimulating expression of c-Fms [29]. Thus, GSD patients may have increased numbers of osteoclast precursors or their osteoclast precursors may have increased potential to form osteoclasts. In 2001, Hirayama et al. examined the frequency of circulating osteoclast precursors and their sensitivity to osteoclastogenic factors in a GSD patient and age/sex-matched controls, demonstrating that no change was detected in the number of precursors, but precursors from this GSD patient formed more osteoclasts in the presence of RANKL and M-CSF[6]. In this early study, the mononuclear cell-rich layer from a Ficoll-Hypaque gradient of peripheral blood cells was used as source of osteoclast precursors. Future studies using cell specific markers such as c-Fms and RANK to better define circulating osteoclast precursors will help to determine if changes in GSD patients occur at the precursor level. Furthermore, if M-CSF is the main pathologic factor for GSD bone loss, we should be able to detect M-CSF levels in serum of GSD patients. This hypothesis can be tested by measuring M-CSF levels in blood of GSD patients and adding M-CSF blocker to GSD serum-osteoclast cultures.

We demonstrated that RANKL is required for LEC conditioned medium-mediated osteoclast formation in vitro, suggesting that M-CSF produced by LECs by itself is not sufficient enough to induce osteoclastogenesis. It will be important to determine cellular source of RANKL in the GSD lesion. RANKL is produced by many cell types including osteocytes and osteoblasts. We did not detect increased RANKL levels in crushed bone samples from LEC-injected tibiae (Figure 5B), suggesting that LECs may not promote RANKL production in bone cells in our model. However, more studies are needed to examine if other cell types in bone of GSD patients express high levels of RANKL to contribute to elevated osteoclastogenesis and bone erosion.

GSD histopathology is composed of osteolysis and vessel formation, including both blood and lymphatic vessels. M-CSF also affects angiogenesis and lymphangiogenesis because M-CSF deficiency is associated with impairment of vascular and lymphatic development [32]. Thus, LEC-produced M-CSF may lead to lymphatic vessel formation after LECs are injected into the bone marrow. We found that LECs express very low levels of M-CSF

receptor c-Fms, suggesting that LEC-produced M-CSF is unlikely to feed back to LECs to promote their proliferation or form lymphatic vessels.

With all available cell specific markers for LECs, we are unable to detect lymphatic vessels in the mouse bone marrow cavity under normal conditions. Thus, an important question will be how are LECs present in the bone marrow of GSD patients? Currently, we do not have an answer. It is possible that stem cells in the bone marrow have the capacity to differentiate to LECs and form lymphatic vessels under certain conditions or LECs may migrate to the bone marrow cavity in response to certain factors. Furthermore, we used an LEC line in most of our experiments despite the fact that we also show M-CSF production by primary LECs. It will be critical to know if LECs from GSD lesions express higher levels of M-CSF than LECs from non-GSD lesions. All these possibilities need to be tested in the future. Another concern is the fate of injected LECs. We found that massive podoplanin+ cells were present within the bone marrow, but lymphatic vessels did not form. Some populations of these podoplanin+ cells within the bone marrow express M-SCF, while others do not. Since LECs were not labeled prior to injection, it is unclear if injected cells remain or if these are endogenous cells; it is also unknown which cells co-express M-CSF. To solve these importance questions, we can label LECs and examine their distribution and fate after tibial injection in the future study. A major challenge of the GSD study is that it is rare, with only about 200 cases reported, making it very difficult to collect a sufficient number of samples or standardize sample-handing by individual investigators. Despite these challenges, our study indicates that LECs could function as effector cells in GSD osteolysis and M-CSF may be a key factor for bone destruction in GSD patients.

In summary, we demonstrated that LECs promote osteoclast formation and bone resorption by producing high levels of M-CSF. Intra-tibial injection of LECs causes massive osteolysis, bone destruction and osteoclast formation, which is attenuated by the M-CSF/c-Fms signal inhibitor Ki20227. Lymphatic vessels in a GSD bone sample are stained positively for M-CSF. Thus, LECs cause bone destruction *in vivo* in mice by secreting M-CSF, which promotes osteoclast formation and activation. Blocking M-CSF signaling may represent a new therapeutic approach for treatment of patients with GSD.

Acknowledgments

References

1. Nikolaou VS, et al. Vanishing bone disease (Gorham-Stout syndrome): A review of a rare entity. World J Orthop. 2014; 5(5):694–8. [PubMed: 25405099]

2. Patel DV. Gorham's disease or massive osteolysis. Clin Med Res. 2005; 3(2):65–74. [PubMed: 16012123]

3. Kiran DN, Anupama A. Vanishing bone disease: a review. J Oral Maxillofac Surg. 2011; 69(1):199–203. [PubMed: 21030127]

4. Devlin RD, Bone HG 3rd, Roodman GD. Interleukin-6: a potential mediator of the massive osteolysis in patients with Gorham-Stout disease. J Clin Endocrinol Metab. 1996; 81(5):1893–7. [PubMed: 8626854]

5. Moller G, et al. The Gorham-Stout syndrome (Gorham's massive osteolysis). A report of six cases with histopathological findings. J Bone Joint Surg Br. 1999; 81(3):501–6. [PubMed: 10872375]

6. Hirayama T, et al. Cellular and humoral mechanisms of osteoclast formation and bone resorption in Gorham-Stout disease. J Pathol. 2001; 195(5):624–30. [PubMed: 11745700]

7. Colucci S, et al. Gorham-Stout syndrome: a monocyte-mediated cytokine propelled disease. J Bone Miner Res. 2006; 21(2):207–18. [PubMed: 16418776]

8. Rohrschneider LR, et al. Growth and differentiation signals regulated by the M-CSF receptor. Mol Reprod Dev. 1997; 46(1):96–103. [PubMed: 8981370]

9. Gillespie MT. Impact of cytokines and T lymphocytes upon osteoclast differentiation and function. Arthritis Res Ther. 2007; 9(2):103. [PubMed: 17381830]

10. Laine CM, et al. WNT1 mutations in early-onset osteoporosis and osteogenesis imperfecta. N Engl J Med. 2013; 368(19):1809–16. [PubMed: 23656646]

11. Prisby R, et al. Intermittent PTH(1–84) is osteoanabolic but not osteoangiogenic and relocates bone marrow blood vessels closer to bone-forming sites. J Bone Miner Res. 2011; 26(11):2583–96. [PubMed: 21713994]

12. Barou O, et al. Relationships between trabecular bone remodeling and bone vascularization: a quantitative study. Bone. 2002; 30(4):604–12. [PubMed: 11934653]

13. von Andrian UH, Mackay CR. T-cell function and migration. Two sides of the same coin. N Engl J Med. 2000; 343(14):1020–34. [PubMed: 11018170]

14. Zhang Q, et al. VEGF-C, a Lymphatic Growth Factor, Is a RANKL Target Gene in Osteoclasts That Enhances Osteoclastic Bone Resorption through an Autocrine Mechanism. J Biol Chem. 2008; 283(19):13491–9. [PubMed: 18359770]

15. Sironi M, et al. Generation and characterization of a mouse lymphatic endothelial cell line. Cell Tissue Res. 2006; 325(1):91–100. [PubMed: 16534603]

16. Ohno H, et al. A c-fms tyrosine kinase inhibitor, Ki20227, suppresses osteoclast differentiation and osteolytic bone destruction in a bone metastasis model. Mol Cancer Ther. 2006; 5(11):2634–43. [PubMed: 17121910]

17. Arnaoutova I, Kleinman HK. In vitro angiogenesis: endothelial cell tube formation on gelled basement membrane extract. Nat Protoc. 2010; 5(4):628–35. [PubMed: 20224563]

18. Takeshita S, Kaji K, Kudo A. Identification and characterization of the new osteoclast progenitor with macrophage phenotypes being able to differentiate into mature osteoclasts. J Bone Miner Res. 2000; 15(8):1477–88. [PubMed: 10934646]

19. Zhang H, Xing L. Ubiquitin e3 ligase itch negatively regulates osteoblast differentiation from mesenchymal progenitor cells. Stem Cells. 2013; 31(8):1574–83. [PubMed: 23606569]

20. Wilting J, et al. The transcription factor Prox1 is a marker for lymphatic endothelial cells in normal and diseased human tissues. FASEB J. 2002; 16(10):1271–3. [PubMed: 12060670]

21. Hirakawa S, et al. Identification of vascular lineage-specific genes by transcriptional profiling of isolated blood vascular and lymphatic endothelial cells. Am J Pathol. 2003; 162(2):575–86. [PubMed: 12547715]

22. Hong YK, et al. Prox1 is a master control gene in the program specifying lymphatic endothelial cell fate. Dev Dyn. 2002; 225(3):351–7. [PubMed: 12412020]

23. Kaipainen A, et al. Expression of the fms-like tyrosine kinase 4 gene becomes restricted to lymphatic endothelium during development. Proc Natl Acad Sci U S A. 1995; 92(8):3566–70. [PubMed: 7724599]

24. Wigle JT, Oliver G. Prox1 function is required for the development of the murine lymphatic system. Cell. 1999; 98(6):769–78. [PubMed: 10499794]

25. Breiteneder-Geleff S, et al. Angiosarcomas express mixed endothelial phenotypes of blood and lymphatic capillaries: podoplanin as a specific marker for lymphatic endothelium. Am J Pathol. 1999; 154(2):385–94. [PubMed: 10027397]

26. Yao Z, et al. Tumor necrosis factor-alpha increases circulating osteoclast precursor numbers by promoting their proliferation and differentiation in the bone marrow through up-regulation of c-Fms expression. J Biol Chem. 2006; 281(17):11846–55. [PubMed: 16461346]

27. Ross FP. M-CSF, c-Fms, and signaling in osteoclasts and their precursors. Ann N Y Acad Sci. 2006; 1068:110–6. [PubMed: 16831911]

28. Xing L, Schwarz EM, Boyce BF. Osteoclast precursors, RANKL/RANK, and immunology. Immunol Rev. 2005; 208:19–29. [PubMed: 16313338]

29. Arai F, et al. Commitment and differentiation of osteoclast precursor cells by the sequential expression of c-Fms and receptor activator of nuclear factor kappaB (RANK) receptors. J Exp Med. 1999; 190(12):1741–54. [PubMed: 10601350]

30. Makinen T, et al. Isolated lymphatic endothelial cells transduce growth, survival and migratory signals via the VEGF-C/D receptor VEGFR-3. Embo J. 2001; 20(17):4762–73. [PubMed: 11532940]

31. Kriehuber E, et al. Isolation and characterization of dermal lymphatic and blood endothelial cells reveal stable and functionally specialized cell lineages. J Exp Med. 2001; 194(6):797–808. [PubMed: 11560995]

32. Kubota Y, et al. M-CSF inhibition selectively targets pathological angiogenesis and lymphangiogenesis. J Exp Med. 2009; 206(5):1089–102. [PubMed: 19398755]

33. Dickson GR, et al. An investigation of vanishing bone disease. Bone. 1990; 11(3):205–10. [PubMed: 2390378]

34. Dellinger MT, Garg N, Olsen BR. Viewpoints on vessels and vanishing bones in Gorham-Stout disease. Bone. 2014; 63:47–52. [PubMed: 24583233]

35. Radhakrishnan K, Rockson SG. Gorham's disease: an osseous disease of lymphangiogenesis? Ann N Y Acad Sci. 2008; 1131:203–5. [PubMed: 18519972]

36. Dupond JL, et al. Plasma VEGF determination in disseminated lymphangiomatosis-Gorham-Stout syndrome: a marker of activity? A case report with a 5-year follow-up. Bone. 2010; 46(3):873–6. [PubMed: 19931435]
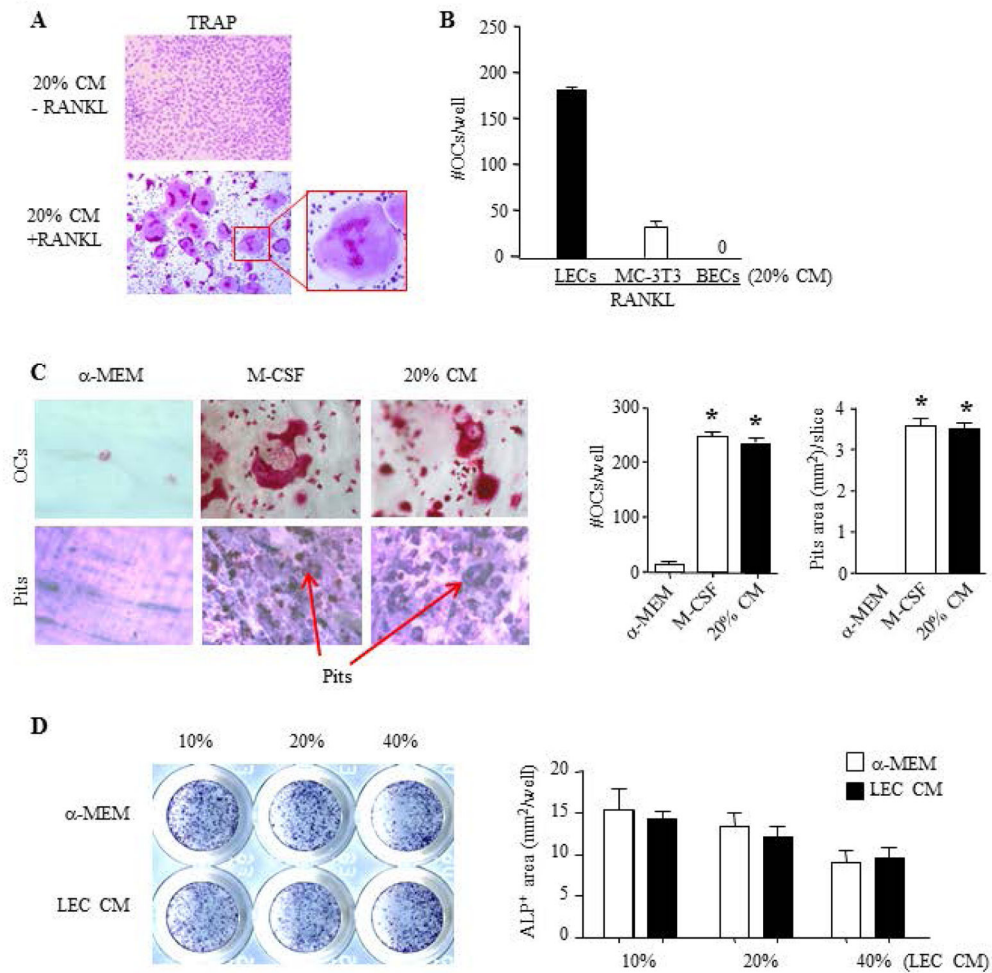
Figure 1. Conditioned media from LECs promote osteoclast formation and bone resorption in vitro

A. WT BM cells were cultured with 20% LEC conditioned media (CM) +/− RANKL for 6 days. TRAP staining was performed for OCs. The insert showing an OC with multiple nuclei.

B. WT BM cells were cultured with 20% CM from LECs, MC-3T3 osteoblast precursors, BECs with RANKL for 6 days. OC numbers were counted. Values are the mean ± SD of 3 wells. Experiments=3

C. WT BM cells were cultured on bone slices with RANKL + 20% CM for 10 days. Bone slices were stained for TRAP activity to identify OCs and with toluidine blue for resorption pits. Values are the mean ± SD of 4 wells. *p<0.05 vs. α-MEM. Experiments=3

D. WT mouse mesenchymal precursor cells were cultured with LEC CM in osteoblast-inducing medium for 2 days. ALP staining was performed. Values are mean ± SD of 5 wells. Experiments=3
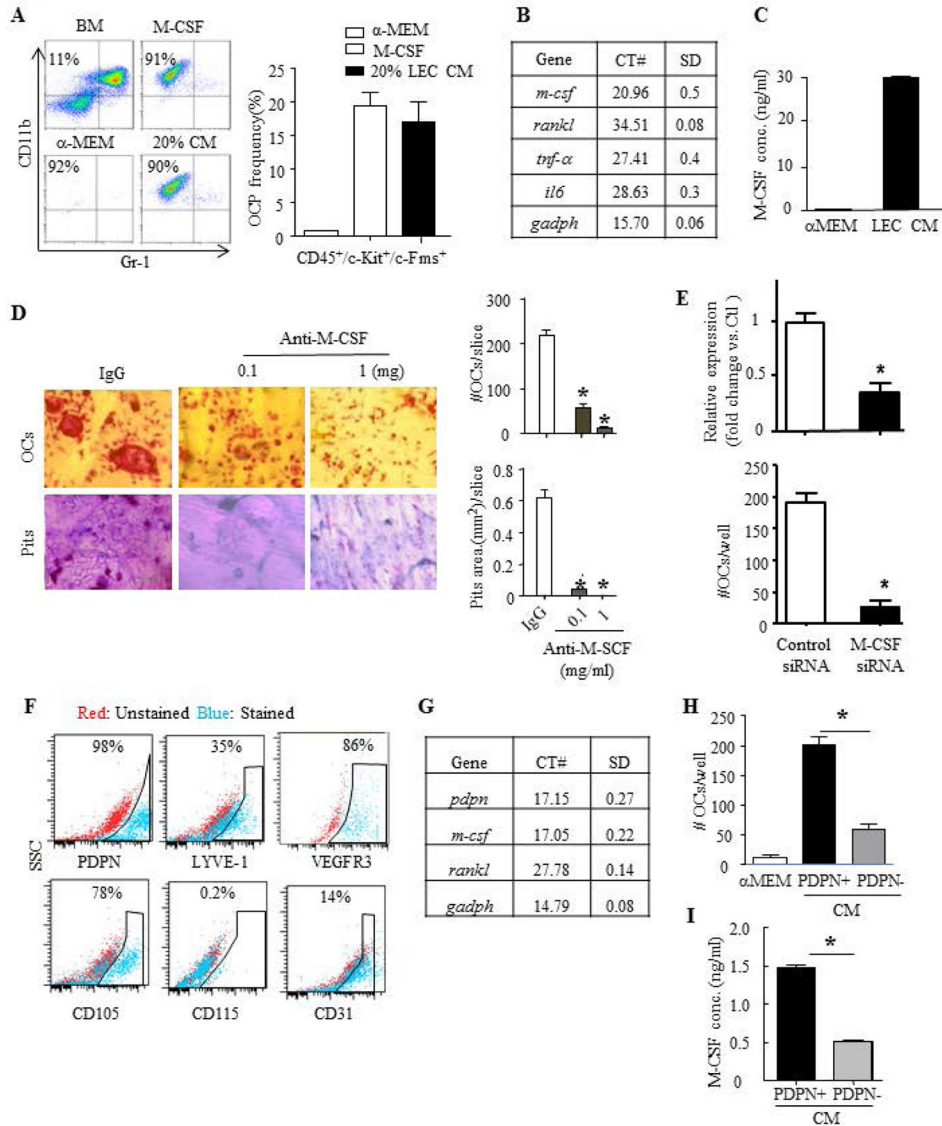
Figure 2. M-CSF produced by LECs stimulate osteoclast formation

A. WT BM cells were cultured with 20% LEC CM for 3 days and % of cells expressing markers for OC precursors were assessed by flow cytometry. Experiments=3

B. Expressions of osteoclastogenic genes by qPCR. Values are the mean ± SD of 3 wells. The CT numbers for each gene were shown. Experiments=3

C. CM M-CSF levels by ELISA. Values are the mean ± SD of 4 wells. *p<0.05 vs. α-MEM. Experiments=3.

D. WT BM cells were cultured on bone slices with RANKL + 20% LEC CM plus IgG or M-CSF neutralizing Ab (=anti-M-CSF) for 10 days. OC numbers and resorption pits area were determined as in Fig. 1. Values are the mean ± SD of 4 wells. *p<0.05 vs. IgG. Experiments=3

E. M-CSF knockdown in LECs was performed with M-CSF siRNA. Expression of M-CSF was determined by qPCR. OC formation by CM from M-CSF and control siRNA-

transfected LECs was examined. OC numbers were counted. Values are the mean ± SD of 4 wells. *p<0.05 vs. control siRNA-transfected cells. Experiments=3

F. Expression of LEC surface markers on primary PDPN+ cells by flow cytometry.

G. Expressions of osteoclastogenic genes in PDPN+ cells by qPCR. Values are the mean ± SD of 3 wells. Relative expression was calculated as in B. Experiments=3

H. WT BM cells were cultured with RANKL + 40% CM from PDPN+ or PDPN− cells to form OCs. OC numbers were counted. Values are the mean ± SD of 4 wells. *p<0.05 vs. PDPN− cells. Experiments=3

I. M-CSF levels by ELISA. Values are the mean ± SD of 4 wells. *p<0.05 vs. PDPN− cells. Experiments=3
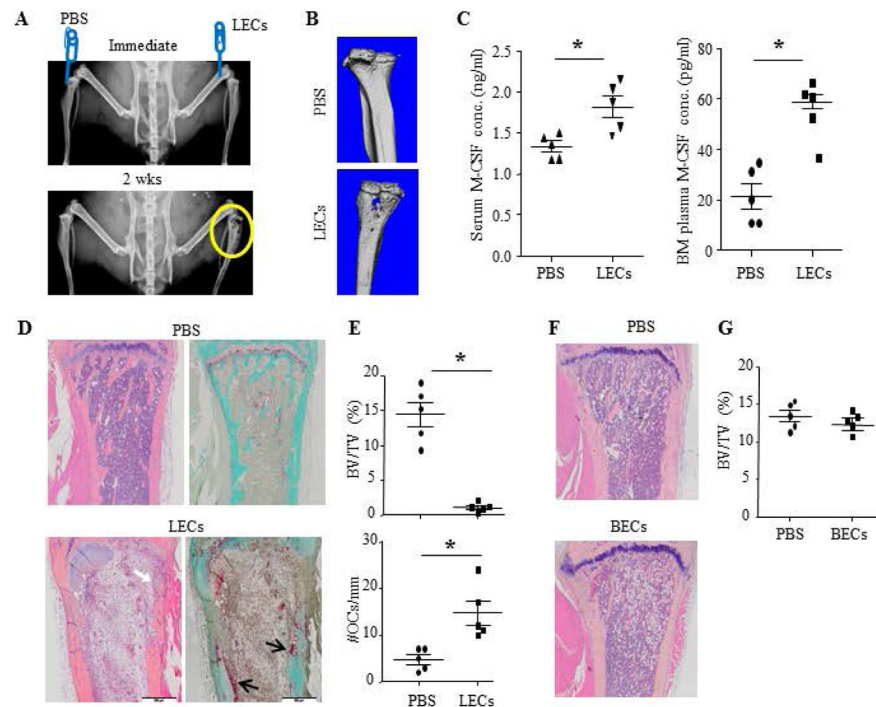
Figure 3. Intra-tibial injection of LECs leads to osteolysis and elevates M-CSF levels in recipient mice

10–week-old WT female mice were used. Right tibiae were injected with LECs (A–E) or BECs (F–G) and left tibiae with PBS. Mice were examined at 2 wks post LEC injection.

A. X-ray showing osteolysis in a LEC-injected tibia.

B. Micro-CT showing bone loss in a LEC-injected tibia.

C. ELISA showing higher M-CSF levels in serum and BM of mice injected with LECs. Values are the data from individual mice (n=5). *p<0.05 vs. PBS-injected mice.

D. H&E- and TRAP-stained images showing trabecular bone loss and cortical bone erosion (white arrow) in a LEC-injected tibia, associated with increased TRAP+ OCs (black arrows).

E. Histomorphometric analysis of H&E- and TRAP-stained sections. Values are the data from individual mice (n=5). *p<0.05 vs. PBS-injected mice.

F. H&E-stained images showing no bone loss in a BEC-injected tibia.

G. Histomorphometric analysis of H&E-stained sections. Values are the data from individual mice (n=5). *p<0.05 vs. PBS-injected mice.
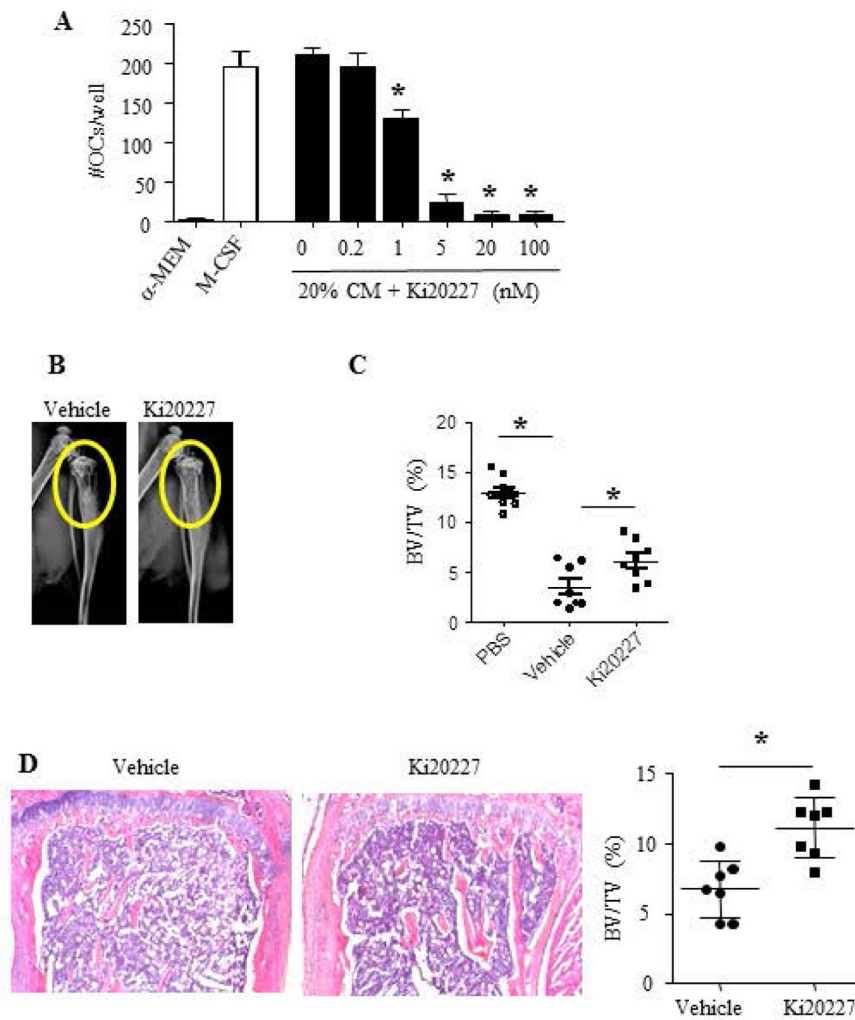
Figure 4. The c-Fms inhibitor, Ki20227, suppresses LEC-induced osteoclastogenesis and osteolysis

A. WT BM cells were cultured with RANKL and 20% LEC CM plus different doses of Ki20227 for 6 days. TRAP staining for OCs was performed. Values are the mean ± SD of 4 wells. *p<0.05 vs. 20% LEC-CM. Experiments=3

B–C. 10–weeks-old female WT mice received intra-tibial injection of LECs were treated with Ki20227 (40 mg/kg/daily) or vehicle (saline) for 2 wks. Micro-CT analysis (C) and histomorphometric analysis of H&E-stained sections (C) show that Ki20227-treated mice displayed reduced bone loss. Values are the data from individual mice (n=7). *p<0.05 vs. vehicle-treated mice.
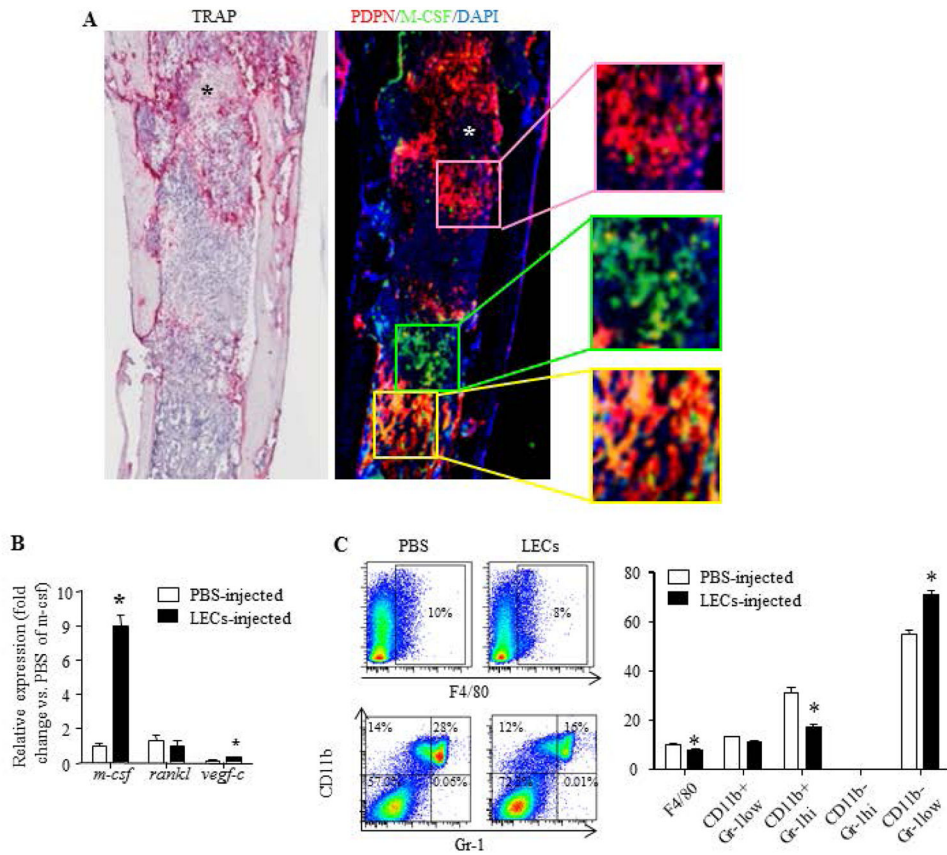
Figure 5. Intra-tibial injected LECs express podoplanin and M-CSF

A. WT mice received an intra-tibial injection of LECs or PBS and were sacrificed 19 days post-injection. Adjacent frozen sections were subjected for TRAP or immune-fluorescent staining with anti-PDPN and M-CSF antibodies. Sections were scanned by the Olympus VS120 whole slide imaging system. Inserts showing PDPN+ (upper panel), M-CSF+ (middle panel) and M-CSF+/PDPN+ cells (lower panel). Experiments=5. *=bone

B. Tibiae were collected at 2 weeks post-LEC injection. Expression of osteoclastogenic genes was examined by qPCR. Values are the mean ± SD of 5 mice. *p<0.05 vs. PBS-injected tibiae.

C. Bone marrow cells were collected from tibiae at 2 weeks post-LEC injection. Alternation of myeloid cells was examined by flow cytometry. Values are the mean ± SD of 5 mice. *p<0.05 vs. PBS-injected tibiae.
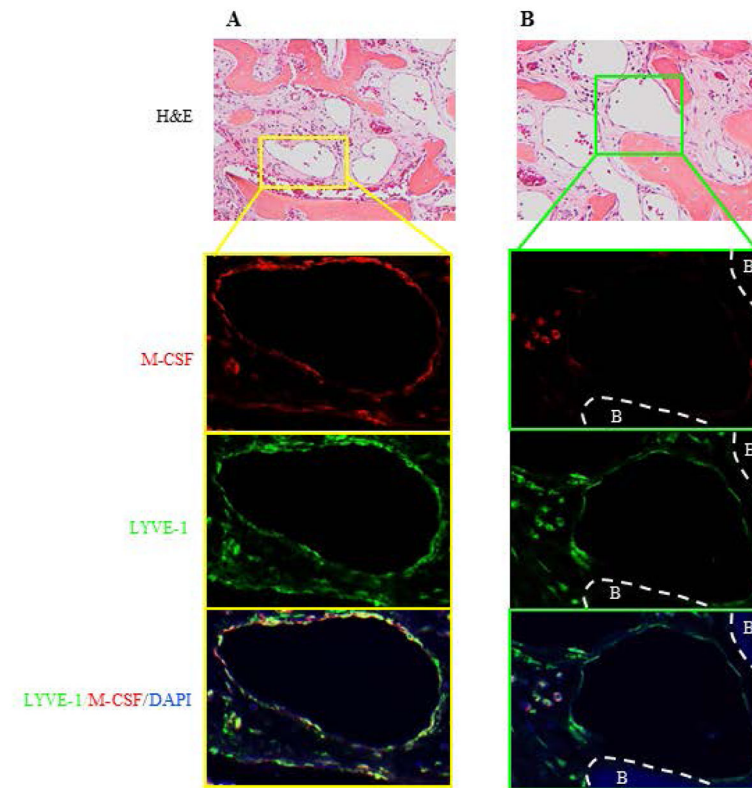
Figure 6. Lymphatic endothelial cells in bone samples from a GSD patient express M-CSF

Paraffin sections of bone sample from a female GSD patient were subjected to H&E (upper panels) and immunofluorescence staining (lower panels) with anti-LYVE-1 and M-CSF antibodies. Stained sections were scanned using an Olympus VS120 whole slide imaging system.

A. Insert showing a LYVE-1+/M-CSF+ lymphatic vessel.

B. Insert showing a LYVE-1+/M-CSF− lymphatic vessel. B=bone

Table

Sequences of Primers Used in the Real-Time Polymerase Chain Reaction

Gene		Sequence of Primer	Accession No.	Product Size (bp)	Locus on gene
mProx1	F 5′-3′	CTTCCGCCATCCCTTTCC	NM_008937	69	1917–1985
	R 5′-3′	CCGGAGGGAGCACCTAGTG			
mLyve1	F 5′-3′	TGGTGTTACTCCTCGCCTCT	NM_053247	214	105–318
	R 5′-3′	TTCTGCCGTGACTCTACCTG			
mPDPN	F 5′-3′	CACCTCAGCAACCTCAGAC	NM_010329	332	564–895
	R 5′-3′	ACAGGGCAAGTTGGAAGC			
mCD31	F 5′-3′	GGAGAGGTTGTCAGAGTTGTTT	NM_001032378	385	61–445
	R 5′-3′	CACCATCGCATCGTCCTTATAG			
mVegfr-3	F 5′-3′	CTGCCTTCAGCTTACCTATAC	NM_008029	351	5236–5586
	R 5′-3′	CTCAATCCCACAGACAGGTTAG			
mVEGF-C	F 5′-3′	CAAGGCTTTGAAGGCAAAG	NM_009506	351	391–782
	R 5′-3′	TGCTGAGGTAACCTGTGCTG			
mTNFa	F 5′-3′	CACACTCAGATCATCTTCTCAA	NM_013693	182	401–582
	R 5′-3′	AGTAGACAAGGTACAACCCATC			
mIL6	F 5′-3′	CTCTGGGAAATCGTGGAAAT	NM_031168	134	253–386
	R 5′-3′	CCAGTTTGGTAGCATCCATC			
mRankL	F 5′-3′	CCAAGATCTCTAACATGACG	NM_011613	140	732–871
	R 5′-3′	CACCATCAGCTGAAGATAGT			
mM-CSF	F 5′-3′	TGTCCTGTCACAAGCTCTGG	NM_001113529	208	2639–2646
	R 5′-3′	AGGGCATCAGAACAAGTTGG			
mGAPDH	F 5′-3′	GGTCGGTGTGAACGGATTTG	NM_008084	675	84–758
	R 5′-3′	ATGAGCCCTTCCACAATG			
mb-actin	F 5′-3′	GTCAGGATCTTCATGAGGTAGT	NM_007393	224	280–503
	R 5′-3′	ACCCAGATCATGTTTGAGAC			